Procedure development for the trajectory reconstruction of a probe descending in a planetary atmosphere: application to Galileo and HASI balloon tests.

V. Gaborit

Laboratoire d'Etudes Spatiales et d'Instrumentation en Astrophysique (LESIA), Observatoire de Paris-Meudon, 5 place Jules Janssen, 92195, Meudon, France.

e-mail: vincent.gaborit@obspm.fr
tel: 00-33-1-45-07-77-19
fax: 00-33-1-45-07-71-10

Abstract

The Huygens probe will enter Titan's atmosphere on January,14th 2005. The probe trajectory reconstruction will be needed to analyse, interpret and correlate all the data taken from each instruments on board Huygens. The Huygens Atmospheric Structure Instrument (HASI) which includes accelerometers, pressure and temperature sensors, will provide essential data to perform an accurate trajectory reconstruction. On the basis of these data, recovered from the HASI sensors, a modular software has been developed at LESIA (Laboratory for Space Studies and Astrophysical Instrumentation) at the observatory of Paris-Meudon. The goals of this software are to perform an accurate trajectory reconstruction during both the entry phase and the descent phase and to deliver the density, pressure and temperature atmospheric profiles throughout the descent. In addition, the choice of a modular configuration facilitates easy implementation for other planetary missions.

Here are presented the algorithms and the method used to reconstruct the probe trajectory during both the entry and the descent phase. This presentation consists in the description of the model used for the probe during the entry and descent configuration, the model used for the planet (gravity field and atmospheric properties) and finally, the set of equations and the integrator scheme used to perform the trajectory reconstruction. This software was tested with the Galileo Atmospheric Structure Instrument data, available in the NASA PDS (Planetary Data System) archives. In addition, three balloon tests were launched in summer 2001, 2002, and 2003 respectively to simulate in the Earth atmosphere the Huygens probe descent. A 1:1 scaled mock-up of the Huygens probe, equipped with HASI spare sensors, was released at 32 km altitude and decelerated by a parachute. Data recovered from the successful 2002 balloon campaign were used to test the developed software and the analysis of the data from the successful 2003 balloon campaign is in progress. The results of these different software tests are presented and discussed.

Introduction

A planetary mission consisting in the descent of a probe in a planetary atmosphere needs an accurate trajectory reconstruction. This trajectory reconstruction gives a reference to analyse correctly all the other data delivered by the instruments on-board the probe. Thus, the trajectory reconstruction has a key role in the success of a planetary mission and has to be treated in a very accurate manner.

Usually, the descent of a probe in a planetary atmosphere consists in two parts. One part is the entry phase, located in the upper and middle atmosphere, during which the probe is protected by a front shield and an after cover. The initial velocity of the probe reaches several km.s^{-1} (about 6 km.s^{-1} and 47 km.s^{-1} for the Huygens and Galileo probe respectively) and the probe has to be protected from the strong thermal fluxes encountered during the peak of deceleration in the middle atmosphere. During this phase, the only available scientific data are those delivered by the accelerometers located inside the probe.

The second part is the descent phase, initiated when the probe reaches the subsonic regim. The front shield and the after cover are released. The probe, decelerated by one or several parachutes, is descending throughout the stratosphere and the troposphere (i.e the lower atmosphere) with all the instrumentation operationnal. During the descent phase, the data dedicated to the altitude reconstruction are temperature and pressure data. The horizontal motion of the probe-parachute system can be reconstructed independently, using data from a Doppler Wind Experiment (mounted aboard the Galileo and Huygens probe, see Bird et al., 1997) or any other imaging instruments as DISR (Descent Imager/Spectral Radiometer, Tomasko et al., 1997).

In the present paper, only the data from Atmospheric Structure Instruments (ASI for Galileo and HASI for Huygens) are used (see Seiff et al., 1998; Fulchignoni et al., 1997). The two phases being very different, they are treated independently. The procedures and models used for the reconstruction of the descent and entry phases are first presented. Then, the reconstruction procedures are tested for two cases: i) the reconstruction of the ascent and descent phases during the HASI 2002 balloon test (Fulchignoni et al., 2003; Gaborit et al., 2003a) and ii) the

global reconstruction of the Galileo probe trajectory in Jupiter's atmosphere.

Models and procedures

Descent phase reconstruction

The reconstruction of the altitude during the descent phase is based on the temperature and the pressure data. The two leading equations are the state equation of a real gas given by

$$\frac{PM}{\rho RT} = 1 + B_2(T)\frac{\rho}{M} \quad (1)$$

and the equation of hydrostatic equilibrium

$$\frac{1}{\rho}\frac{\partial p}{\partial z} = -g_v \quad (2)$$

P, T and ρ are respectively the pressure, the temperature and the density of the atmospheric gas. M is the mean molecular mass, $R = 8.314$ $J.K^{-1}.mol^{-1}$ the universal gas constant and B_2 the second virial coefficient of the gas. g_v is the vertical component of the effective gravitationnal field calculated in the planetary rotating frame (including the Coriolis and centrifugal forces) and z is the altitude.

Using equations 1 and 2, the altitude is reconstructed using the vertical velocity equation:

$$\begin{aligned} \triangle z_i &= v_{z,i}(t_i - t_{i-1}) \\ &= -\frac{RT_{i-\frac{1}{2}}(1 + B_2(T)\frac{\rho}{M})}{Mg_v}\ln(\frac{P_i}{P_{i-1}}) \end{aligned} \quad (3)$$

The subscript i is relative to a value obtained at the mission time t_i. v_z is the vertical velocity of the probe-parachute system. The temperature is assumed to be constant between times t_{i-1} and t_i, equal to $T_{i-\frac{1}{2}} = \frac{T_{i-1}+T_i}{2}$.

The equation 3 shows that the mean molecular mass and the second virial coefficient have to be determined accurately. This determination requires the knowledge of the chemical composition which is given with a good accuracy by instruments like GCMS (Huygens Gas Chromatograph and Mass Spectrometer, Niemann et al., 1997) or the PMS (Galileo Probe Mass Spectrometer, Niemann et al., 1998). B_2 coefficients are recovered from the litterature (Dymond and Smith, 1980).

The term g_v in equation 3 requires a model for the gravitationnal field, including the knowledge of the planet angular velocity Ω. The gravitationnal field is modelled using a development in spherical harmonics (Mooij, 1991) and retaining only even terms (i.e. symmetry respect to the equatorial plane). Only harmonics J_2 and J_4 are considered. The influence of a third body is neglected for the Earth and Jupiter case.

The last term of equation 3, $\ln(\frac{P_i}{P_{i-1}})$ (or equivalently the obtained $\frac{dP}{dt}$ profile), requires an accurate treatment for pressure data. In fact, the pressure in both case is acquired with a sampling rate of almost 2 s, and two consecutive values are very close. Now, considering the noise inherant in the measurement, the pressure sensor resolution is not high enough to recover a smooth $\frac{dP}{dt}$ profile. The $\frac{dP}{dt}$ profile has then to be fitted adequately to retrieve a realistic vertical velocity profile (see below for the Earth and Jupiter case).

To take into account the dynamical effects, temperature and pressure data have to be corrected using the two following equations:

$$T_{stat} = \frac{T_{meas}}{1 + [(\gamma_{ad} - 1)/2]Ma^2} \quad (4)$$

$$P_{stat} = P_{meas}(1 + \frac{\gamma_{ad} - 1}{2}M_a^2)^{\frac{\gamma_{ad}}{1-\gamma_{ad}}} \quad (5)$$

where T_{stat} and P_{stat} are the static temperature and pressure, T_{meas} and P_{meas} are the measured one. $\gamma_{ad} = \frac{C_p}{C_v}$ is the ratio of the heat capacities and Ma is the Mach number.

Finally, the reconstruction is performed using a simple Euler integrator, because the vertical velocity profile reconstruction does not imply any "long-life" propagation of errors: the velocity determined at t_i is independant of the one determined at t_j, $|i - j| > 2$.

Entry phase reconstruction

The reconstruction of the entry phase is totally different of the one described for the descent phase. As the only data received during the entry phase are the accelerometer data, the trajectory reconstruction is now based on the equations of motions derived from the Newtonian laws. The six equations of motion expressed in the planet rotating frame are given below:

$$\left\| \begin{array}{l} \dot{V} \\ -V\dot{\gamma} \\ -V\cos(\gamma)\dot{\chi} \end{array} \right. = C_3(-\gamma)C_2(\chi)C_1(\tfrac{\pi}{2}) \left\| \begin{array}{l} a_e \\ a_n \\ a_r \end{array} \right. +$$

$$\frac{V^2}{r}\cos(\gamma) \left\| \begin{array}{l} 0 \\ 1 \\ \cos(\gamma)\cos(\chi)\tan(\delta) \end{array} \right. +$$

$$\Omega^2 r\cos(\delta) \left\| \begin{array}{l} \sin(\gamma)\cos(\delta)+\cos(\gamma)\sin(\chi)\sin(\delta) \\ \cos(\gamma)\cos(\delta)-\sin(\gamma)\sin(\chi)\sin(\delta) \\ \sin(\delta)\cos(\chi) \end{array} \right. +$$

$$2\Omega V \left\| \begin{array}{l} 0 \\ \cos(\delta)\cos(\chi) \\ \sin(\delta)\cos(\gamma)+\sin(\gamma)\sin(\chi)\cos(\delta) \end{array} \right. \tag{6}$$

and

$$\left\| \begin{array}{l} r\dot{\varphi}\cos(\delta) \\ r\dot{\delta} \\ \dot{r} \end{array} \right. = V \left\| \begin{array}{l} \cos(\gamma)\cos(\chi) \\ \cos(\gamma)\sin(\chi) \\ -\sin(\gamma) \end{array} \right. \tag{7}$$

C_i are the standard rotation matrices. a_e, a_n and a_r are the components of the global acceleration of the probe in the local frame (see figure 1). r, δ and φ are respectively the radial position of the probe respect to the center of mass of the planet, the latitude and the longitude (respect to the prime meridian). V is the module of the velocity $\mathbf{V}$ expressed in the rotating frame. γ and χ are defined on figure 1. Ω is the planet angular velocity. These equations are integrated by using a standard Runge-Kutta method.

As seen in the previous equations, the important point for the entry reconstruction is the determination of the global acceleration. The acceleration can be split in two contributions: the gravitationnal and the aerodynamic one. The gravitationnal contribution is calculated with the model described in the previous section and the aerodynamic contribution is directly given by accelerometer measurements. Assuming i) a small value for the angle of attack α of the probe during the entry phase and ii) a coning motion of the probe induced by this angle of attack, the aerodynamic deceleration a_a can be approximated by the relation:

$$\begin{aligned} \mathbf{a}_a &= \frac{\mathbf{F}_D}{m_{pr}} \\ &= \left[cos(\alpha)a_x - sin(\alpha)\left(a_y^2+a_z^2\right)^{1/2}\right]\frac{\mathbf{V}}{V} \end{aligned} \tag{8}$$

where F_D is the drag force and m_{pr} the mass of the probe. a_x (negative), a_y and a_z are respectively the axial and the two lateral accelerations measured by the accelerometer.

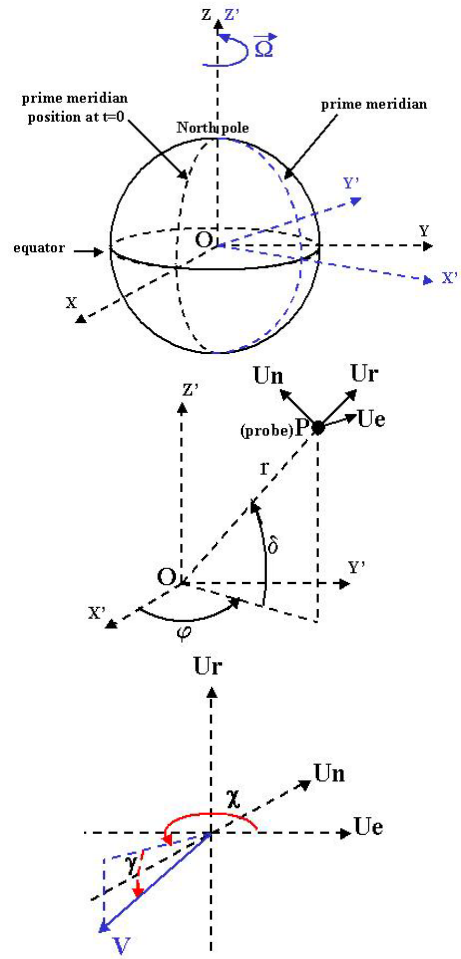

Figure 1: **left**: planet rotating frame (O,X'Y'Z') respect the fixed inertial frame (O,XYZ).-**center**: the local frame and the position variables r, δ and φ.-**right**: velocity variables respect to the local frame.

Thanks to the measurements obtained from the accelerometer, it is possible to derive the density profile. The density is connected to the acceleration by the following relation:

$$a_i = \frac{\rho V^2 C_i S_o}{2m_{pr}} \qquad \text{i=x,y,z} \tag{9}$$

where S_o is the cross section of the probe. The aerodynamic coefficients C_i are determined by both tunnel tests and simulations and depend on the Knudsen (Kn), Reynolds (Re) and Mach number. These coefficients depend also on the attack angle of the probe. Re and Ma depend respectively on the dynamic viscosity and the sound speed, implying an "a priori" knowledge of the upper atmosphere's P-T profile and chemical composition.

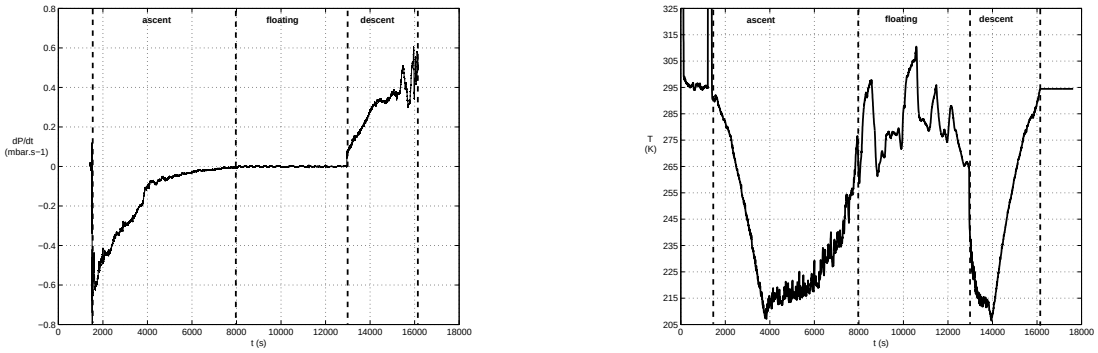

Figure 2: (**left**): smoothed $\frac{dP}{dt}$ profile obtained during the whole flight.-(**right**): temperature profile obtained during the whole flight.

Thanks to the recovered density profile, the pressure profile is reconstructed assuming the hydrostatic equilibrium and the temperature profile is deduced by means of the ideal gas law. The use of the ideal gas law implies also the knowledge of the upper atmosphere's chemical composition.

Using an adequate P-T profile (see below for Jupiter's case), the chemical composition is derived integrating the equation of diffusion (chamberlain, 1987):

$$\begin{aligned}\phi_i &= -n_i D_i\Big(\frac{1}{n_i}\frac{\partial n_i}{\partial z}+\frac{1}{H_i}+\frac{1}{T}\frac{\partial T}{\partial z}\Big)\\ &\quad - n_i K\Big(\frac{1}{n_i}\frac{\partial n_i}{\partial z}+\frac{1}{H}+\frac{1}{T}\frac{\partial T}{\partial z}\Big) \qquad (10)\end{aligned}$$

ϕ_i is the local vertical flux of the i-th constituent, n_i its number density, H_i its pressure scale height, and D_i its molecular diffusion coefficient in the surrounding gas. K is the eddy diffusion coefficient and H is the atmospheric pressure scale height.

Ascent and descent reconstruction for the HASI 2002 balloon test

The data recovered during the HASI 2002 balloon test were used to test the reconstruction procedure for the descent phase. This reconstruction is explained by Gaborit et al. (2003a) and only the final results are presented here.

The $\frac{dP}{dt}$ profile obtained from pressure data is presented figure 2-left. As the $\frac{dP}{dt}$ signal was very noisy, it was smoothed using a running average on 16 data or on 8 s (sampling rate: 2 Hz). Then, this profile was integrated to retrieve a smoothed pressure profile adequate to derive the vertical velocity profile. The temperature profile used for the reconstruction is shown figure 2-right.

The assumptions and parameters used for the reconstruction are:

- the atmospheric gas is well describe by the ideal gas law ($B_2(T)\frac{\rho}{M} \sim 0$).
- the atmospheric gas is in hydrostatic equilibrium.
- $M = 28.96$ g.mol^{-1}, $\gamma_{ad} = 1.4$, $\Omega = 7.2921\times10^{-5}$ rad.s^{-1} and $J_2 = 1.08\times10^{-3}$.

Figure 3-(left) shows the difference Δz between the derived altitude and the altitude provided by the on-board GPS system during the whole flight. This difference is set to 0 at the beginning of the flight. The difference obtained during the ascent phase is very small and is increasing when the altitude is reaching about $18-20$ km. This increase can be attributed to unaccuracies in GPS data above the altitude of 18 km. In fact, it is the maximum altitude for a nominal functionning of non-military GPS receivers. During the descent phase, the difference Δz is different than the one observed during the ascent phase. That means that there is an additionnal source of error for the reconstruction of the descent.

The analysis of the attitude of the probe-parachute sytem (Gaborit et al. 2003b) shows that the mean pendular motion was very strong, leading to inclinations between 20° and 40° during the first 300 s of the descent phase. This strong pendular motion induced dynamical effects which did pertubate the pressure measurements, during the first 300 s of the descent or for altitudes between 22 and 32 km (see figure 3-(right)). This period corresponds exactly to

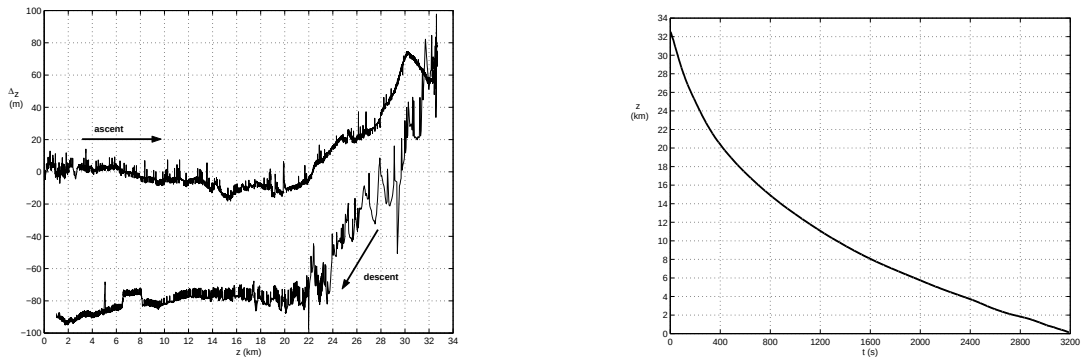

Figure 3: **left**: difference Δz between the derived altitude and the one given by the GPS system during both the ascent and the descent phases.-**right**: reconstructed altitude (in km) versus descent time (in s). The time is set equal to 0 at probe release.

the strong decrease of Δz at the beginning of the descent phase.

At the end of the descent, the global difference is about 160 m (+70 m at the beginning of the descent and −90 m at the end), if GPS unaccuracies are included. Then the relative error is very small and less than 0.5% for the whole descent. Consequently, the reconstruction procedure seems to be very accurate for the descent phase.

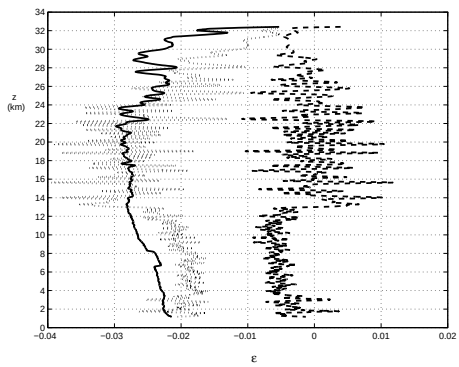

Figure 4: relative error ϵ on the pressure (solid line), the temperature (dashed line) and the density (dotted line) for the descent reconstruction.

The figure 4 shows the corresponding relative error on the density, the pressure and the temperature during the whole descent. In this case too, the mean relatives errors are very small: less than 3% for the pressure and the density and less than 1% for the temperature.

Entry and Descent reconstruction using Galileo data.

The descent of the Galileo probe in Jupiter's atmosphere can be divided in three sequences:

- the entry phase with a mission time t between −240.555 and 0 s.
- a connexion phase ($0 < t < 16.2$ s) during which the only data available is an average of the acceleration during the period $0.02 < t < 16$ s. This phase has to be simulated, taking into account the different events (parachute opening, after cover and front shield release).
- the descent phase for $t > 16.2$ s.

The navigation team of the Galileo mission gave very accurate initial conditions corresponding to the altitude 450 km above the 1 bar level. But the mission time was not well determine (1 σ error: 26 s). Consequently, to have an altitude reference, the reconstruction of the trajectory of the probe has to be initiated by the descent phase reconstruction to set the reference at the 1 bar level. Then, the connexion phase is simulated. Finally, the entry phase is reconstructed taking into account the constraints given by the navigation data and by the reconstruction of the descent and connexion phases.

Descent phase

The descent phase is reconstructed using the three available sets of pressure data P1, P2 and P3, and the two available sets of temperature data T1 and T2 (see Seiff et al., 1998; PDS data archive). The corresponding $\frac{dP}{dt}$ and temperature profiles used for the reconstruction are presented figure 5.

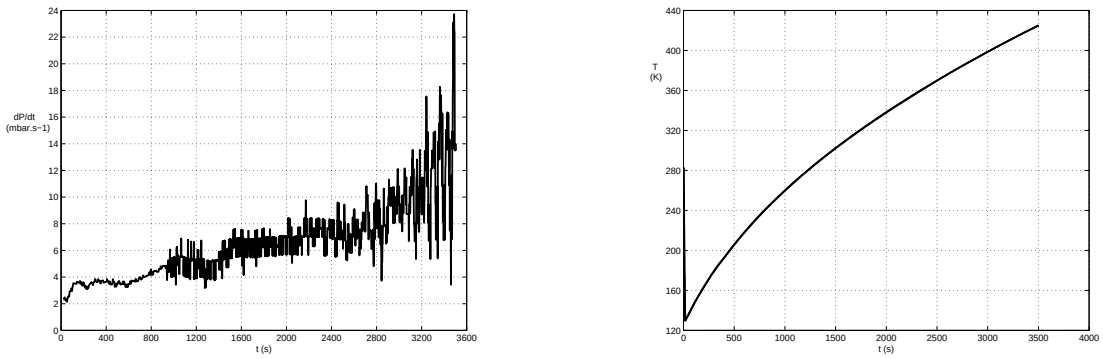

Figure 5: **left**: smoothed $\frac{dP}{dt}$ profile for the descent phase -**right**: temperature profile during the descent phase.

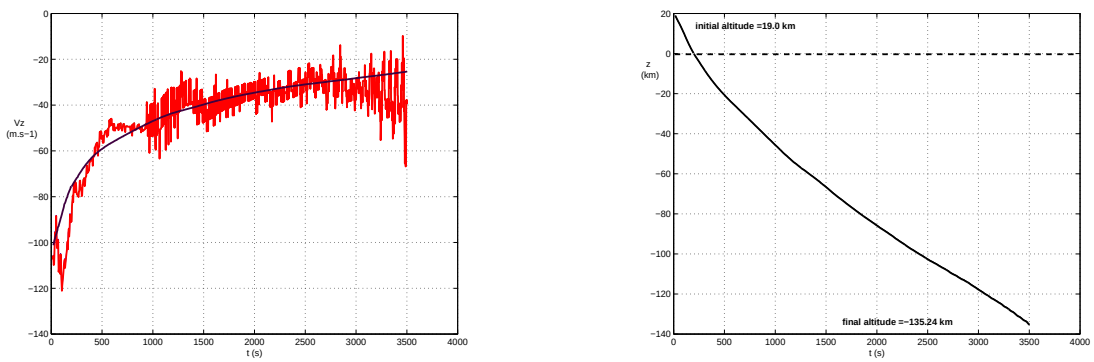

Figure 6: **left**: vertical velocity (in m.s^{-1}) versus time (in s) during the descent phase. The dark line shows the theoretical terminal speed.-**right**: deduced altitude profile (in km) versus time (in s).

As explained before, this $\frac{dP}{dt}$ profile was obtained by smoothing the raw profile with a running average on 5 data for the P2 signal and on 10 data for P3 signal, which is more scattered.

To achieve the reconstruction, the mean molecular mass was derived from the chemical composition determined from the PMS (Niemann et al., 1998). The real gas equation was used, with a second virial coefficient determined considering only the two major constituent H_2 and He. The hydrostatic equilibrium is assumed and the gravitationnal field is modelled considering these parameters: $J_2 = 1.4736 \times 10^{-2}$, $J_4 = -5.89 \times 10^{-4}$, $\Omega = 1.7585 \times 10^{-4}$ rad.s^{-1}, Jupiter's mass $M_j = 1.8986 \times 10^{27}$ kg and Jupiter's equatorial radius at $P = 1$ bar $R_J =$ 71492 km. The 1 bar level is considered to be an ellipsoid with the excentricity $e = 0.35430$.

Figure 6 present the reconstructed vertical velocity profile (left) and the deduced altitude profile (right). The theoretical terminal speed of the probe-parachute system is also shown. The two profiles are in good agreement, if we consider that the differences are due to complex dynamics, except at the end of the descent. In fact the pressure measurements were perturbated by the high pressures encountered, and the velocity profiles is increasing slowly showing strong oscillations. Consequently, the altitude profile determined for $t > 3000$ s may be perturbated and slightly underestimated.

The descent phase reconstruction shows that the initial altitude and vertical speed at $t = 16.2$ s are about 19.0 km and 107.3 m.s^{-1} respectively. The density at this point is equal to 9.495×10^{-2} kg.m^{-3}.

Connexion phase

Using the averaged deceleration of the probe between 0.02 and 16 s (i.e. 42.901 m.s^{-2}), the velocity of the probe can be determined for $t = 0$ s, and we find $V \simeq 426.8$ m.s^{-1}. Then, it is possible to simulate the vertical velocity profile and the corresponding altitude profile during this phase, considering the following events:

-$t = 0$ s, descent mode detection,

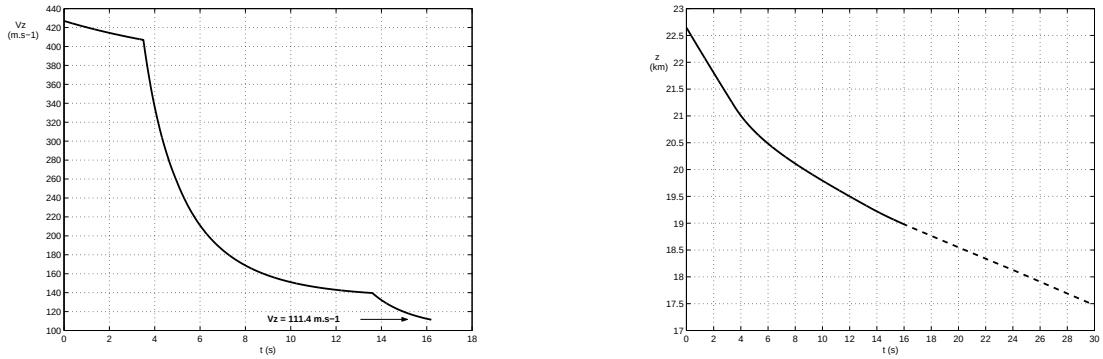

Figure 7: **left**: vertical velocity (in m.s^{-1}) versus time (in s) during the connexion phase.-**right**: deduced altitude profile (in km) versus time (in s).

Table 1 - values for m_s in kg (probe-parachute system mass), $C_{x,pr}$, $C_{x,pa}$ (probe and parachute aerodynamic coefficients), $S_{o,pr}$ et $S_{o,pa}$ in m^2 (probe and parachute cross section) versus time.

t (s)	$0-3.5$	$3.5-5$	$5-13.6$	$13.6-16.2$
m_s	241	241	230	121
$C_{x,pa}$	0	0.464	0.464	0.464
$C_{x,pr}$	0.74	0.74	0.74	0.8
$S_{o,pr}$	1.14	1.14	1.14	0.61
$S_{o,pa}$	0	11.40	11.40	11.40

-$t = 3.5$ s, parachute opening,
-$t = 5$ s, after cover release,
-$t = 13.6$ s, front shield release,
and assuming that the velocity of the probe is given by the vertical velocity (i.e. $\sin(\gamma) \simeq 1$). The table 1 shows all the parameters used in this simulation.

Figure 7 shows the velocity (left) and the altitude (right) profiles during this connexion phase.

The altitude profile shows that the conditions at $t = 0$ are $z = 22.6$ km and $V = 426.8$ m.s^{-1}.

Entry phase

Knowing the conditions at $t = 0$, the entry phase was first reconstruct upward to estimate the altitude of the probe when the first data is acquiered ($t = -240.555$ s). Then, several reconstructions were performed to match exactly the conditions (at 450 km) delivered by the navigation team.

The reconstruction is using an upper atmosphere P-T profile based on the ISO-SWS observations (Drossard et al., 1998) to model the upper atmosphere chemical composition (eddy coefficient at the homopause $K_h = 7.10^{-2}$ m^2.s^{-1}, with a dependance in $n^{-0.5}$). The molecular diffusion coefficients for each species are found in the litterature (Marrero and Masson, 1972; Kestin et al., 1984). The lower atmosphere composition used to derive the chemical composition at high altitude is restricted to the main constituents (H_2, He, CH_4 and H). Figure 8 shows the molecular fraction used for the reconstruction.

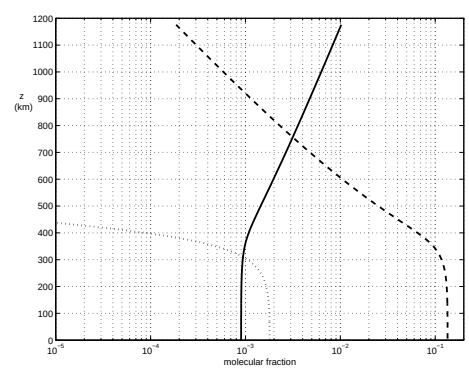

Figure 8: Molecular fraction of He(dashed-line), H (solid-line) and CH_4 (dotted-line) versus altitude.

For the entry reconstruction, the exospheric temperature T_{ex} has to be assumed. That is why four reconstructions were performed, with $T_{ex} = 700$, 900, 1100 and 1200 K respectively.

The probe model is described figure 9. The upper-left and upper-right graphs show the C_x coefficient used for the reconstruction. The bottom-left and bottom-right graphs show the evolution of the mass and radius of the probe, due to the mass ablation during the entry.

The acceleration data used for the reconstruction are provided by two axial sensors (a_1 and a_2) and two orthogonal lateral sensors (a_n).

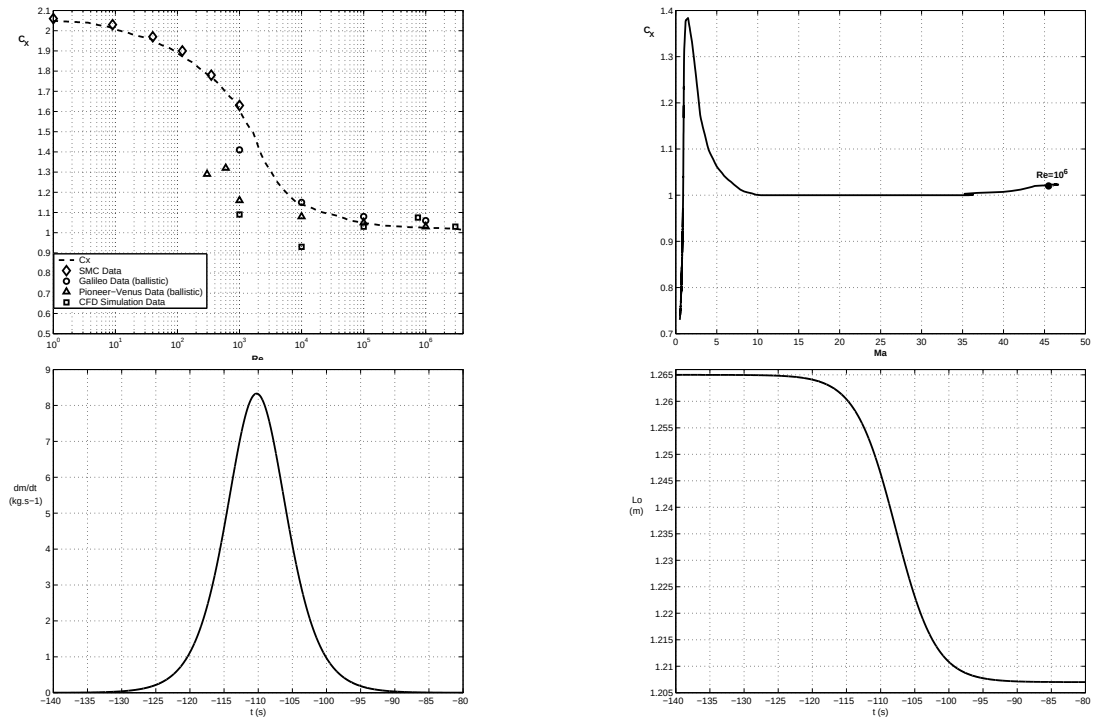

Figure 9: **upper-left/right**: variation of C_x with Re and Ma.-**bottom left/right**: evolution of the probe mass ($\frac{dm}{dt}$ profile) and probe radius with time.

These data are shown figure 10. Data a_1 and a_2 are in very good agreement. Consequently the acceleration profile used for the reconstruction is an average of the two profiles. The angle of attack can not be derived before $t = -160$ s, because the resolution of the lateral sensors is not high enough.

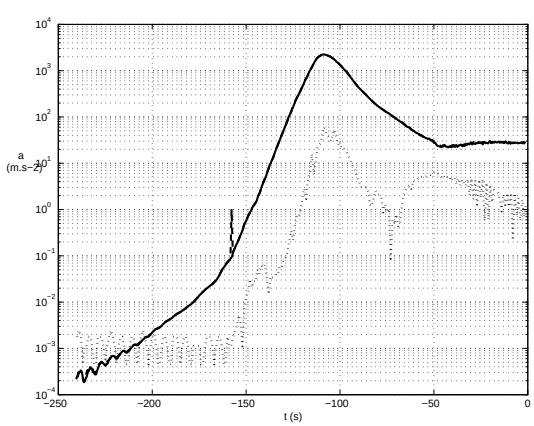

Figure 10: Acceleration data obtained from the two axial sensors (dashed and solid line), and normal acceleration retrieved from the lateral sensors (dotted line)

The final result of the reconstruction is given table 1 and figures 11, 12 and 13, for the entry trajectory, the density, pressure and temperature profiles respectively.

The result of the entry reconstruction is in excellent agreement with i) the navigation data and ii) with the conditions expected at the beginning of the descent phase. The obtained γ angle at $t = 0$ confirms the assumption made for the connexion phase: $\sin(\gamma) = 0.993 \simeq 1$. The calculated angle of attack α remains small, except during the transonic regime with a maximum value of about 17.6^o. But the approximation made of small angle of attack remains valid. As the winds were neglected, the real φ and δ values at the end of the entry may be different from those shown in table 2.

Concerning the density, pressure and temperature profiles, the agreement between the entry phase and the descent phase is excellent too. In fact, a simple extrapolation of the descent profile allows a perfect connexion with the entry profile. The density profile shows some fluctuations at the end of the entry due to instabilities in the aerodynamic coefficients during the subsonic regime. The sudden change in the slope observed above the homopause, is probably due

Table 2- results for the entry trajectory reconstruction.

t (s)	z (km)	V (m/s)	γ (^{o})	χ (^{o})	φ (^{o})	δ (^{o})	α (^{o})
-240.555	**1039.00**	**47123.6**	**10.6549**	**-2.0924**	**2.1501**	**6.6442**	-
-234.930	990.22	47146.8	10.4871	-2.1314	2.3575	6.6366	-
-229.305	942.16	47169.7	10.3191	-2.1704	2.5653	6.6289	-
-223.680	894.84	47192.3	10.1511	-2.2094	2.7733	6.6209	-
-218.055	848.27	47214.6	9.9829	-2.2484	2.9818	6.6129	-
-212.430	802.43	47236.5	9.8147	-2.2874	3.1905	6.6047	-
-206.805	757.34	47258.1	9.6463	-2.3263	3.3996	6.5963	-
-201.180	713.00	47279.3	9.4779	-2.3653	3.6090	6.5878	-
-195.555	669.41	47300.2	9.3093	-2.4042	3.8187	6.5791	-
-189.930	626.57	47320.8	9.1407	-2.4431	4.0287	6.5703	-
-184.305	584.48	47341.0	8.9720	-2.4820	4.2390	6.5613	-
-178.680	543.15	47360.8	8.8031	-2.5209	4.4496	6.5522	-
-173.055	502.57	47380.3	8.6342	-2.5597	4.6606	6.5429	-
-167.430	462.75	47399.3	8.4652	-2.5986	4.8718	6.5334	-
-165.606	**450.00**	**47405.4**	**8.4104**	**-2.6111**	**4.9403**	**6.5303**	-
-161.805	423.68	47418.0	8.2961	-2.6374	5.0832	6.5238	-
-156.180	385.37	47436.0	8.1270	-2.6762	5.2950	6.5140	2.076
-150.555	347.85	47452.7	7.9577	-2.7149	5.5070	6.5041	2.318
-144.930	311.08	47465.5	7.7884	-2.7536	5.7193	6.4940	2.071
-139.305	275.08	47467.3	7.6191	-2.7924	5.9318	6.4838	0.608
-133.680	239.88	47422.5	7.4499	-2.8310	6.1444	6.4734	0.137
-128.055	205.53	47201.3	7.2816	-2.8696	6.3567	6.4629	0.104
-122.430	172.29	46339.0	7.1170	-2.9080	6.5669	6.4524	0.171
-116.805	140.90	43605.7	6.9652	-2.9456	6.7700	6.4421	0.389
-111.180	113.46	35858.3	6.8553	-2.9814	6.9511	6.4328	0.805
-105.555	93.32	23718.8	6.8613	-3.0133	7.0852	6.4258	1.101
-99.930	80.65	13985.9	7.0816	-3.0422	7.1684	6.4214	1.400
-94.305	72.89	8144.6	7.6403	-3.0721	7.2168	6.4189	1.035
-88.680	67.75	5118.3	8.6876	-3.1075	7.2458	6.4173	0.560
-83.055	63.87	3425.7	10.3699	-3.1521	7.2646	6.4163	0.400
-77.430	60.63	2413.7	12.8540	-3.2097	7.2774	6.4156	0.680
-71.805	57.74	1737.4	16.3430	-3.2850	7.2864	6.4151	0.481
-66.180	55.07	1283.3	21.0701	-3.3848	7.2928	6.4147	2.434
-60.555	52.50	994.8	27.1210	-3.5163	7.2975	6.4144	7.828
-54.930	49.93	819.4	34.2521	-3.6859	7.3010	6.4142	12.190
-49.305	47.29	712.5	41.9504	-3.9002	7.3037	6.4140	17.577
-43.680	44.53	666.0	49.4853	-4.1630	7.3059	6.4139	13.121
-38.055	41.60	636.0	56.3392	-4.4801	7.3076	6.4137	9.075
-32.430	38.59	608.0	62.3860	-4.8685	7.3091	6.4136	9.180
-26.805	35.57	575.3	67.6394	-5.3564	7.3102	6.4135	3.906
-21.180	32.62	541.2	72.1576	-5.9875	7.3111	6.4134	2.795
-15.555	29.79	507.5	75.9780	-6.8219	7.3117	6.4134	3.695
-9.930	27.09	475.2	79.1515	-7.9477	7.3122	6.4133	2.370
-4.305	24.53	449.0	81.7187	-9.4794	7.3125	6.4133	1.715
-2.430	23.70	440.1	82.4511	-10.1062	7.3126	6.4132	1.965
-1.180	23.16	434.1	82.9083	-10.5629	7.3127	6.4132	1.531
0	**22.64**	**428.4**	83.3399	-10.9940	7.3128	6.4132	-

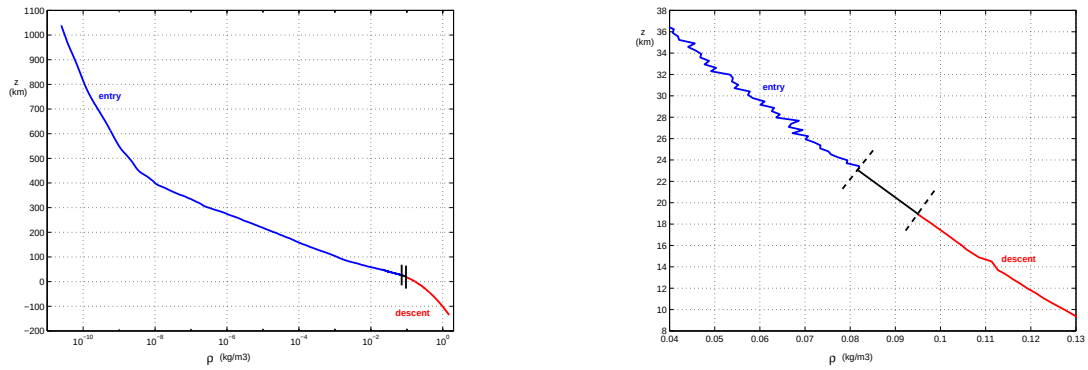

Figure 11: **left**: density profile for the whole reconstruction.-**right**: zoom on the connexion phase.

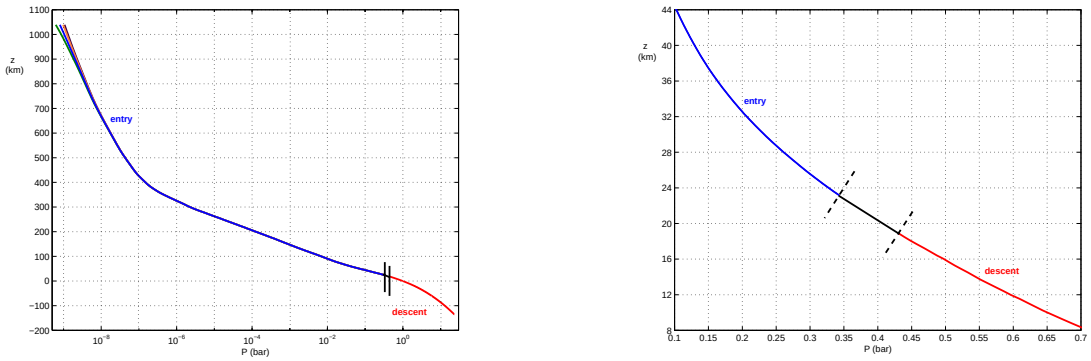

Figure 12: same figure for the pressure profile.

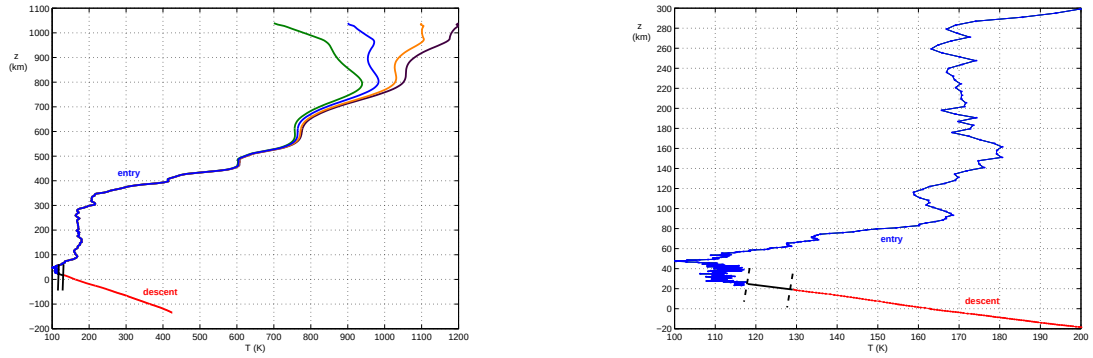

Figure 13: same figure for the temperature profile.

to gravity waves dissipations which are inducing a strong temperature gradient (Yelle et al., 1996; Seiff et al., 1998). These features can be observed in the upper atmosphere's temperature profiles.

Concerning the pressure and temperature profiles, four curves corresponding to the four different exospheric temperatures are represented. These curves converge quickly, depending only on the ratio between the initial difference in pressure and the pressure at a given level.The convergence is better than 11% at 800 km and less than 1% at 500 km. The shape of the pressure profile is almost the same as the one of the density profile.

The temperature profile shows five main parts:

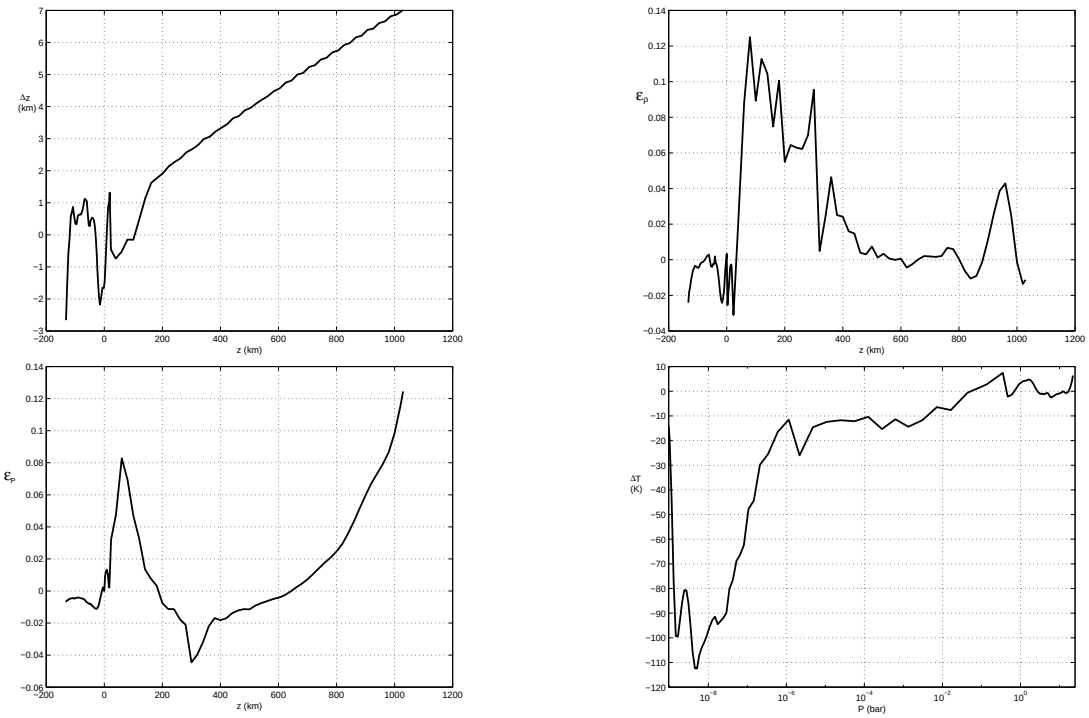

Figure 14: Difference between the presented profiles and those derived by Seiff et al. (1998). **upper-left**: difference in altitude (km) versus time (in s).-**upper-right**: relative difference ϵ_ρ in density versus altitude.-**bottom-left**: relative difference ϵ_P in pressure versus altitude.-**bottom-right**: difference in temperature ΔT versus altitude.

a near adiabatic troposphere, a small near-isothermal layer between 25 and 55 km, a strong stratospheric gradient between 55 and about 100 km, a deep isothermal layer ($T \simeq 170$ K) between 140 and 280 km and finally an upper atmosphere with strong temperature gradient and gravity waves.

All these results are very similar to those presented by Seiff et al. (1998). The figure 14 shows the difference between the profiles presented in this paper and those derived by Seiff et al. (1998).

Except for the temperature in the upper atmosphere, the differences remain small. The altitude shows a difference of about 6 km for the entry phase which represents a discrepancy smaller than 1%. Some significant variations can be observed around the pic of deceleration because during this period, the reconstruction is very sensitive to any small discrepancies in any parameters. Those variations propagate naturally in the pressure and density profiles.

The main difference between the two sets of results is due to the treatment of the connexion phase. In fact, Seiff et al. inferred a variation in altitude of about 6 km during this phase, which has to be compared to the 3.68 km value for this reconstruction.

The difference between the temperature profile increases with decreasing pressure and is probably due to the different upper atmosphere model (i.e. the eddy diffusion coefficient) used for the reconstruction. It is quite interesting to see the influence of the upper atmosphere model on the reconstructed temperature profile.

Conclusion

The reconstruction using data of the HASI 2002 balloon test and those from the Galileo probe have shown that the procedures developped for the future analysis of the Huygens mission are valid and give very consistant results.

The altitude reconstruction for the HASI balloon test provides an accuracy of about 0.5% for the whole descent, this accuracy being probably surestimated if we consider the additionnal uncertainties introduced by GPS data at high altitude. This study confirms also the very high quality of data sets provided by the HASI experiment. This result is very interesting in anticipation of the Huygens mission if we consider

that the accuracy can be of the same order in Titan's atmosphere.

The trajectory reconstruction of the Galileo probe is a very good test because the available data are typically the same as those which will be delivered by the HASI experiment. The very good consistancy of the reconstruction (entry-connexion-descent) shows that the developped procedures have good performance and are suitable for such an analysis.

In the next few months, this work will be optimized for the Huygens mission. On the one hand, the models which give the loss of data due to the new definition of the Huygens mission, have to be considered. On the other hand, new observations of Titan (Titan occultation in November 2003 and Titan observations by Cassini at the end of 2004) should provide additionnal informations on Titan's atmosphere properties.

References

Bird, M.K., Heyl, M., Allison, M., Asmar, S.W., Atkinson, D.H., Edenhofer, P., Plettemeier, D., Wohlmuth, R., Iess, L., Tyler, G.L., The Huygens Doppler Wind Experiment, *ESA SP 1711*, 139-162, 1997.

Chamberlain, J.W., Hunten, D.M., Theory of planetary atmopsheres, *Academic Press*, 1987.

Drossard, P., Fouchet, T., Crovisier, J., Lellouch, E., Encrenaz, T., Feuchtgruber, H., and Champion, J.-P., Fluorescence in the 3 micron bands of methane on Jupiter and Saturn from ISO/SWS observations, *Proceedings of the ISO Paris Conference: "the universe as seen by ISO"*, October 1998.

Dymond J.H., and Smith, E.B., The virial coefficients of pure gases and Mixtures, A critical compilation, *Oxford University Press*, Oxford, 1980.

Fulchignoni, M., Angrilli, F., Bianchini, G., Bar-Nun, A., Barucci, M.A., Borucki, W., Coradini, M., Coustenis, A., Ferri, F., Grard, R.J., Hamelin, M., Harri, A.M., Leppelmeier, G.W., Lopez-More-no, J.J., McDonnell, J.A.M., McKay, C., Neubauer, F.H., Pedersen, A., Picardi, G., Pirronello, V., Pirjola, R., Rodrigo, R., Schwingenschuh, C., Seiff, A., Svedhem, H., Thrane, E., Vanzani, V., Visconti, G., Zarnecki, J.C., The Huygens Atmospheric Structure Instrument (HASI), *ESA SP 1711*, 163-176, 1997.

Fulchignoni, M., Aboudan, A., Angrilli, F., Antonello, M., Bastianello, S., Bettanini, C., Bianchini, G., Colombatti, G., Ferri, F., Flamini, E., Gaborit, V., Ghafoor, N., Hathi, B., Harri, A-M., Lehto, A., Lion Stoppato, P.F., Patel, M.R., Zarnecki, J.C., A stratospheric balloon experiment to test the Huygens Atmospheric Structure Instrument (HASI), *Pl. Sp. Sci.* (submitted), 2003.

V. Gaborit, M. Fulchignoni, G. Colombatti, F. Ferri and C. Bettanini, Huygens/HASI 2002 balloon test campaign : probe trajectory and atmospheric vertical profiles reconstruction, *Planet. Sp. Scie.* accepted, 2003a.

Gaborit, V., Antonello, M., Colombatti, G., Fulchignoni, M., HASI 2002 balloon campaign : Probe-Parachute system attitude analysis, *J. of Aircraft* submitted, 2003b.

Kestin, J., Knierim, K., Mason, E.A., Najafi, B., Ro, S.T., and Waldman, M., Equilibrium and Transport Properties of the Noble Gases and Their Mixtures at Low Density, *J. Phys. Chem. Ref. Data*, 13, 229, 1984.

Marrero, T.R., and Mason, E.A., Gaseous diffusion coefficients, *J. Phys. Chem. Ref. Data*, 1,3, 1972.

Mooij E., Developpement of START, a Six Degrees of Freedom Simulation Tool for Atmospheric Re-entry Trajectories, *ESTEC W. P. 1633*, October 7, 1991.

Niemann, H., Atreya, S., Bauer, S.J., Biemann, K., Block, B., Carignan, G., Donahue, T., Frost, L., Gautier, D., Harpold, D., Hunten, D., Israel, G., Lunine, J., Mauersberger, K., Owen, T., Raulin, F., Richards, J., Way, S., The Gas Chromatograph Mass spectrometer aboard Huygens, *ESA SP 1711*, 85-107, 1997.

Niemann, H.B., Atreya, S.K., Carignan, G.R., Donahue, T.M., Haberman, J.A., Harpold, D.N., Hartle, R.E., Hunten, D.M., Kasprzak, W.T., Mahaffy, P.R., Owen, T.C., and Way, S.H., The composition of the Jovian atmosphere as determined by the Galileo probe mass spectrometer, *J. Geophys. Res.*, Volume 103, Issue E10, pp. 22831-22846., 1998.

Seiff, A., Kirk, D.B., Knight, T.C.D., Young, R.E., Mihalov, J.D., Young, L.A., Milos, F.S., Schubert, G., Blanchard, R.C., and Atkinson, D.H., Thermal structure of Jupiter's atmosphere near the edge of a 5-μm hot spot in the north equatorial belt, *J. Geophys. Res.*, Vol. 103, n° E10, 22857-22889, 1998.

Tomasko, M.G., Doose, L.R., Smith, P.H., West, R.A., Soderblom, L.A., Combes, M., Bézard, B., Coustenis, A., de Berg, C., Lellouch, E., Rosenqvist, J., Saint-Pé, O., Schmitt, B., Keller, H.U., Thomas, N., Gliem, F., The Descent Imager/Spectral Radiometer (DISR) aboard Huygens, *ESA SP 1711*, 109-138, 1997.

Yelle, R.V., Young, L.A., Vervack Jr., R.J., Young, R.E., Pfister, L., and Sandel, B.R., Structure of Jupiter's upper atmosphere : Predictions for galileo, *J. Geophys. Res.*, 101(E1), 2149-2161, 1996.